Analysis of the Effect of Different Helmet Types and Conditions in Two Real-world Accident Scenarios with a Human Body Model

Desiree Kofler, Ernst Tomasch, Peter Spitzer, Corina Klug

Abstract In the current study, head impacts from real-world moped crashes were analysed to evaluate the influence on injury outcome of different helmet geometries and unfastened chinstraps in primary and ground impacts. Finite element simulations of real-world moped to car crashes were conducted based on technical reports providing initial conditions for two crash scenarios. Finite element helmet models of a full-face and a motocross helmet were generated and validated on the basis of drop test data. The THUMS v4 was equipped with the different helmets and positioned on a moped model. In a parameter study, the influence of helmet type and unfastened chinstrap was evaluated in primary and ground impacts.

The analysis of the different helmet types showed increased neck loadings and relative displacements between head and helmet due to the lever effect of the protruding chinguard of the motocross helmet. All simulations involving a loose chinstrap resulted in helmet loss, consequently leading to increasing the head injury severity in the ground impact.

Both helmet models correlated sufficiently with the reference to drop test data. The parameter study on helmet geometry as well as chinstrap conditions revealed that these factors influence the injury outcome.

Keywords FE helmet model, human body model, moped accident simulation.

I. INTRODUCTION

More than 3,800 moped riders are involved in accidents on Austrian roads every year [1]. The most frequently injured body regions are the upper and lower extremities, followed by the head if considering absolute values. In relative values related to the Abbreviated Injury Scale (AIS), head injuries predominate in the AIS3+ level, as seen in European studies [2], as well as in Austrian databases [3]. Despite 100% compliance with statutory helmet regulation, head injuries are still observed in moped accidents. Compared to other Vulnerable Road Users (VRUs) [4–11], significantly fewer studies are available on the analysis of injury mechanisms with detailed Human Body Models (HBMs) of moped riders [12-13].

Within a pre-study for the current analyses, moped accidents involving moped riders between the ages of 15-17 in Graz, Austria, were recorded over a period of one year (2017). It was observed that this age group favours motocross helmets, which are related to a slightly higher risk of head and neck injuries than full-face helmets. However, the sample sizes were too small to achieve statistical significance. The researchers also observed that one third of the interviewed moped riders had not fitted the chinstrap properly.

The present study aimed to investigate the above findings within a numerical study under realistic boundary conditions. As these effects cannot be studied in conventional helmet testing due to limitations in load cases and injury assessment, the influence of helmet geometries and chinstrap fit have been investigated by means of simulations with a detailed HBM in crash scenarios based on real-world accidents.

In the current study, head impacts from moped crashes with realistic boundary conditions were analysed, and the following questions have been discussed:

- How does helmet geometry influence injury outcome in real-world accident conditions?
- Does an unfastened chinstrap affect the impact and injury outcomes in real-world accident conditions?
- Is the severity of the ground impact worse than the primary vehicle impact?

II. METHODS

To answer these questions, finite element (FE) simulations based on real-world moped to car accidents were set up and simulated. Furthermore, a parameter study on helmet geometry was conducted and the influence of the chinstrap evaluated in primary and ground impacts.

D. Kofler (email: desiree.kofler@tugraz.at; tel: +43 316 873 30350) is research assistant, E. Tomasch is senior scientist and C. Klug is assistant professor at the Vehicle Safety Institute of Graz University of Technology, Austria. P. Spitzer is scientific director at the research Center for Childhood Accidents, Safe Kids Austria, Graz, Austria.

Derivation of Crash Scenarios based on Real-world Accidents

The first step involved determining accident scenarios by identifying relevant accidents held on the Austrian Central Database for In-Depth Accident Study (CEDATU), for in-depth analysis of national road accidents [3]. All data sets can be filtered according to several accident characteristics such as accident type, collision partner or injury levels.

To determine, which accidents would be suitable for investigating the questions discussed here, the database was filtered for cases involving at least one moped rider. Single-vehicle accidents were excluded due to unclear boundary conditions. From the remaining datasets, two different impact scenarios representing two different accident types were selected. As 33% of all accidents held on the CEDATU database involve crossroad accidents and 23% had occurred in oncoming traffic [3], one scenario of each type was chosen for the herein conducted study.

The selected scenarios are listed in Table I. Scenario A represents a crossing accident in which the moped rider enters from the right and turns left. The moped rider collides with a sport utility vehicle (SUV) at an angle of 60°, which continues straight through the crossroad. The impact is located at the right front tyre of the SUV. Scenario B involves a frontal collision between a moped and a sedan. The moped rider impacts the sedan with a 90mm offset to the centre of the vehicle at a 10° angle. The collision velocities of the accident opponents were retrieved from the technical reports, which are based on PC-Crash (DSD, Linz, Austria) accident reconstructions.

TABLE I
OVERVIEW OF THE SCENARIOS DERIVED FROM REAL-WORLD ACCIDENTS

	Accident type	Moped velocity [kph]	Vehicle velocity [kph]	Impact angle [°]	Impact location relative to centre on vehicle front [mm]	Vehicle type
Crash Scenario A		37	45	60	x = -420 y = 780	SUV
Crash Scenario B	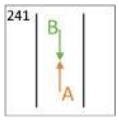	40	90	10	x = 0 y = -90	Sedan

FE Helmet Models

FE models of two different helmet types were developed in order to analyse the influence of helmet geometry. A full-face and a motocross helmet were chosen, as they differ in geometry and are commonly worn by moped riders. Two helmets from the same manufacturer, one of each type, were selected and digital scans of the helmets were generated. The scans provided information on the geometry and served as input for the model generation process. Material properties were adopted from previous simulations comprising bicycle helmets [14]. The outer hard shell was modelled with shell elements and plastic material formulation. The Expanded Poly-Styrene (EPS) liner was assigned a strain rate dependent foam material based on [14] and has been modelled with solid elements connected to the outer liner. However, the comfort foam layer has not been modelled. The element edge lengths of each model were chosen to meet an element edge length of 5mm [15]. The chinstrap is represented by seatbelt elements and constrained via slip rings to the head models. This modelling method was preferred, as it represents a proper chinstrap fit and ensured the helmet was kept in place throughout the simulation. The friction coefficient at the slip rings was set to 0.3 in accordance with the mean value for belt friction derived in [16].

In order to validate the helmet models, a test matrix was set up to test both helmets in several load directions followed by drop tests. The helmets were oriented to impact to the front, rear and left side. Based on standard helmet test regulations, a drop velocity of 7.5m/s was defined [17]. As shown in Fig. 1, the helmets were dropped on a flat anvil as well as a 45° inclined anvil to generate both translational as well as rotational loading. A Hybrid III dummy head was equipped with three-axis acceleration and rotational velocity sensors in the centre of gravity and positioned inside the helmet.

Rear 0° Side 0° Front 0° Side 45° Front 45°

Fig. 1. Test Configurations for helmet drop tests.

The data from the measurements served as input for the validation process. The test setups were simulated with both helmet models and acceleration and rotational velocity curves were compared to the corresponding test data. The correlation between the models and the tests was quantified through Correlation and Analysis (CORA) rating. Thereby, the curve correspondence was evaluated through a corridor method as well as a correlation method, the scores of which add up to the overall score. The evaluation was conducted with the CORA tool implemented in the programme Visual Environment (ESI Group, Paris, France) [18]. Standard settings were retained for the score calculation, which can be found in TABLE A2 of the Appendix. Additionally, injury criteria such as Head Injury Criteria (HIC), Brain Injury Criteria (BrIC) and the maximal resultant acceleration were calculated based on test and simulation data, and subsequently compared.

Accident Simulations with Human Body Model

The 50th percentile THUMS v4.02 [15] was used to represent the moped rider. The THUMS was positioned on a generic moped model, in which the frame of the moped was modelled with beams, by means of pre-simulations. To enable interaction with the THUMS, the tyres, seat and handlebar were modelled with shell elements. Furthermore, the THUMS was equipped with the validated helmet models connected with the aid of a simple-modelled chinstrap using seatbelt elements. Freely available car models were utilised as collision opponents in both simulated accidents [19]. To represent the impact with a SUV, a model of a Toyota RAV 4 was used, while the sedan was represented by a Ford Taurus model.

The simulations were set up with respect to the available data retrieved from the technical reports. In the process, characteristics were established for the initial velocities of the opponent vehicles, impact locations and angles together with the vehicle types. Automatic surface-to-surface contact definitions between the THUMS, helmet, moped and vehicle model, were used to reproduce realistic kinematic behaviour. All simulations were performed in LS-DYNA (DYNAmore, Stuttgart, Germany) with the solver version R9.2.1 MPP.

The simulations injury assessment was comprised exclusively of injury values related to the body regions head and neck. Brain injuries were evaluated by the calculation of the Cumulative Strain Damage Measure (CSDM). CSDM describes the percentage of brain elements exceeding a strain value of 25% [20]. Skull fracture was detected by the 99th percentile strain value exceeding the limit of 1.5% for cortical bone fracture [24-25]. As the strain values have not been validated for the skull, the HIC was derived additionally [21-22] as well as the calculation of the corresponding AIS3+ risk [23]. In order to return head acceleration values, an additional nodal output was implemented at the centre of gravity of the head, constrained to the skull bone. The value a3ms was calculated to compare maximal resultant accelerations, operating for a duration of three milliseconds. To evaluate the loadings on the neck, a cross-section was implemented at the height of the C1 vertebra to output resultant forces and moments acting on the neck.

The rotation and displacement of the helmet compared to the THUMS head was measured at the time of head impact. Therefore, sagittal and transverse planes were established within the helmet and the head model, illustrated in Fig. 2. By measuring the angle between the sagittal planes of the head and helmet (green), the relative rotation of the helmet about the vertical axis was derived. To obtain the relative rotation about the transverse axis, the angle between the transverse planes of the head and helmet (blue) was measured.

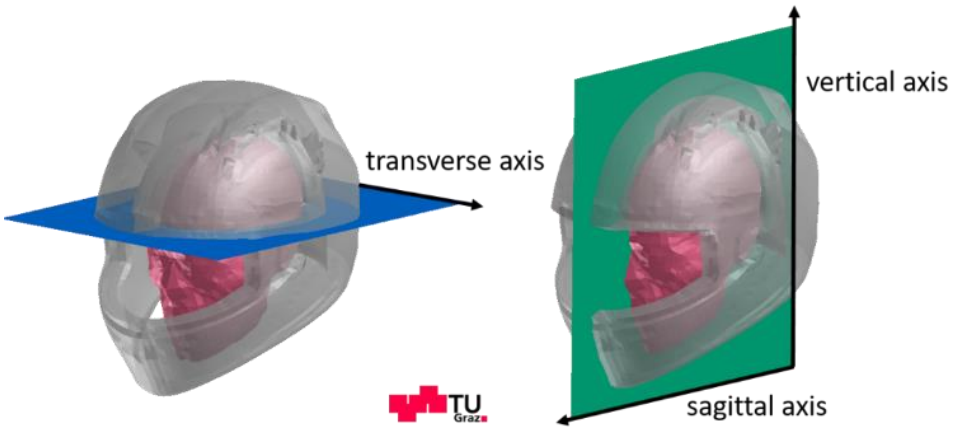

Fig. 2. Sagittal and transverse planes for measurement of relative rotation.

Parameter Study

Table II lists all variations performed for each accident scenario. The simulation comprising the helmet worn by the moped rider in the real-world crash represents the baseline simulation and has been marked bold in the table. In the first step of the parameter study, the helmet type and consequently the geometry of the helmet was varied by implementing the motocross helmet. What effect the protruding chinguard would have on the injury risk was analysed through altering the motocross helmet by extending the chinguard.

In further simulation variations, the effect of an unfastened chinstrap was evaluated with the baseline helmet. To understand the effects of this particular misuse condition, simulations with the full-face helmet, chinstrap fastened and unfastened, were run until ground impact. Hence, facilitated separate evaluation of the primary and ground impacts. The ground impact simulation without chinstrap for Scenario B terminated due to an error prior to ground impact and was therefore deemed unsuitable for evaluation.

The relative comparison of the calculated injury values based on the baseline and modified simulations provided insights as to how injury outcome is affected by these variations.

TABLE II
LIST OF SIMULATIONS FOR THE PARAMETER STUDY

Crash Scenario	Variation
Crash Scenario A	**Full-face helmet**
	Motocross helmet
	Motocross helmet with extended chinguard
	Full-face helmet with unfastened chinstrap
	Full-face helmet (Ground impact)
	Full-face helmet with unfastened chinstrap (Ground impact)
Crash Scenario B	**Full-face helmet**
	Motocross helmet
	Motocross helmet with extended chinguard
	Full-face helmet with unfastened chinstrap
	Full-face helmet (Ground impact)

III. RESULTS

FE Helmet Models

The helmet models were developed by meshing the geometry obtained from digital scans and validated in reference to the drop tests. The validation of the helmet models is demonstrated with one test case of the motocross helmet. The results of the remaining tests can be found in Fig. A1 - Fig. A20 of the Appendix.

Fig. 2 shows the kinematics of the motocross helmet at the lateral drop test on a flat anvil. The visual inspection of the test footage and simulation results show good correspondence in helmet deformation and dummy head rotation.

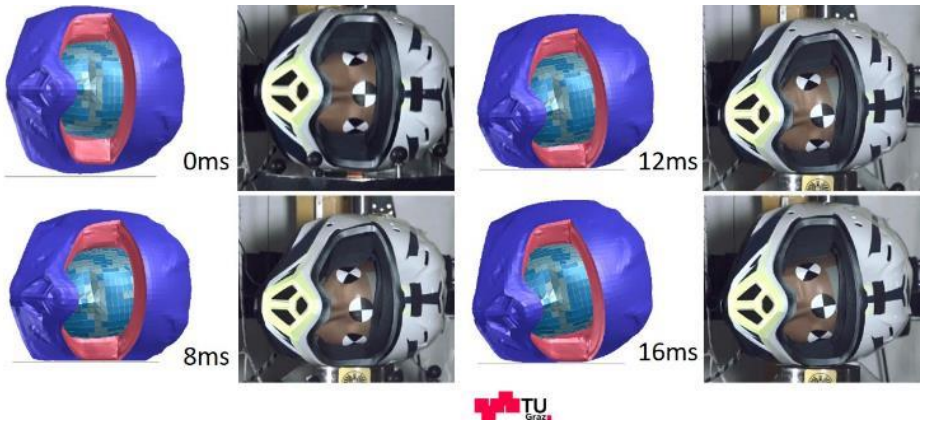

Fig. 2. Comparison of the kinematics: Motocross helmet – lateral – flat anvil.

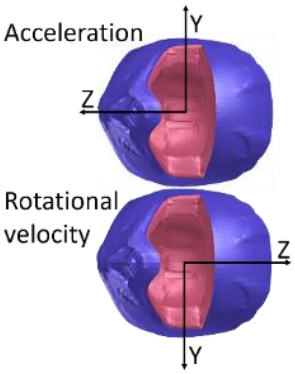

Fig. 3. Coordinate systems of the measured data.

The acceleration and rotational velocity curves recorded during the drop tests were measured in the respective coordinate systems depicted in Fig. 3. The coordinate systems differ, due to the mounting orientation of the sensors. In Fig. 4, the acceleration and rotational velocity curves of the treated example case are illustrated. Despite behaving slightly stiffer at the beginning, good correlation of the curves from the test and simulation has been noted.

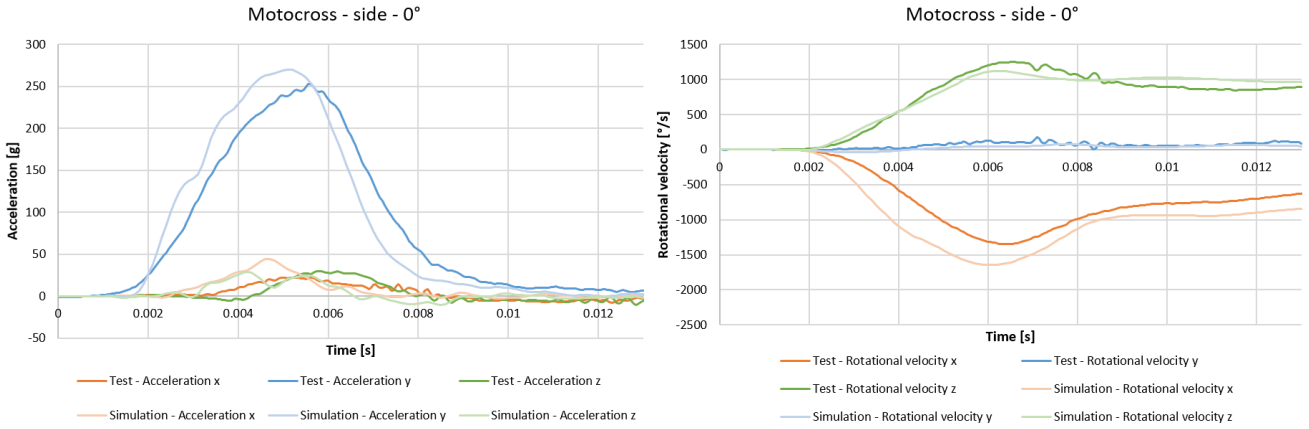

Fig. 4. Acceleration and rotational velocity curves: Motocross helmet – lateral – flat anvil.

The comparison of the calculated injury criteria is listed in Table III. The peak resultant acceleration fits the test by a difference of 24g, which equals a deviation of 9%. The HIC 15 and BrIC values show a deviation of 22% and 14%, respectively. The results of all drop tests are listed in TABLE A3 - TABLE A4 of the Appendix.

TABLE III
COMPARISON OF INJURY CRITERIA OF TEST AND SIMULATION: MOTOCROSS HELMET – LATERAL – FLAT ANVIL

Injury criteria	Drop test	Simulation	Deviation	Deviation [%]
Peak acceleration	253 g	277 g	24 g	9
HIC 15	2342	2847	505	22
BrIC	0.5459	0.4679	-0.078	14

Fig. 6 illustrates the CORA evaluation curves for the lateral drop test of the motocross helmet. The acceleration curve from the simulation and the acceleration curve from the corresponding test are highlighted in red and black, respectively, while the two corridors based on the test curve are highlighted in blue and green. Fig. 7 summarises the CORA scores for the discussed evaluation case. The fit of the curve from the simulation into the corridors was scored with 0.772 points and the correlation method evaluated the fit of the curve shape with 0.8 points. Each score weighted with 50% resulted in an overall score of 0.786. The acceleration and rotational velocity curves and the CORA results of all cases can be found in Fig. A1 - Fig. A20 of the Appendix.

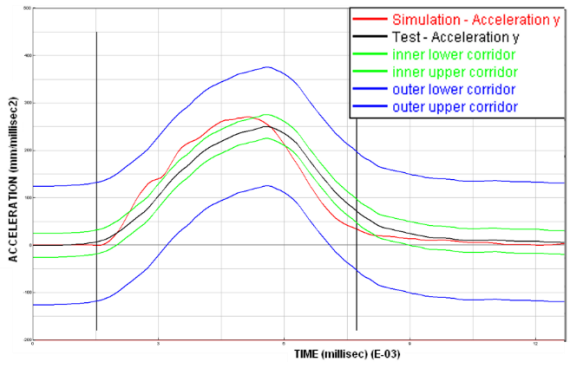

Fig. 5. Curves for the CORA rating of the acceleration curve in y: Motocross helmet – lateral – flat anvil.

No.	Name				Rating	Weight
1	Corridor Method				0.772	0.5
2	Correlation method	Value	Rating	Weight	0.8	0.5
a	Cross correlation function	0.9965	0.9948	0.2		
b	Size	0.8977	0.8977	0.4		
c	Phase shift	0.0004	0.6047	0.4		
3	Combination of 1 and 2				0.786	
	Overall Rating:	**0.786**				

Fig. 6. CORA rating of the acceleration curve in y: Motocross helmet – lateral – flat anvil.

The summary of the CORA ratings for all validation cases can be found in Table A1 of the Appendix. The helmet validation approached mostly good CORA ratings with values above 0.7. Certain validation cases showed poor ratings with values between 0.3 and 0.5 points, mostly occurring at the full-face helmet validation.

Accident Simulations with Human Body Model

The simulations based on the two chosen real word crashes were set up using the validated helmet models, the positioned THUMS v4 as well as the moped and vehicle models. Fig. 7 shows the initial configuration of the two accident scenarios. In both cases, the moped riders wore a full-face helmet in the real-world case, which was therefore taken as baseline.

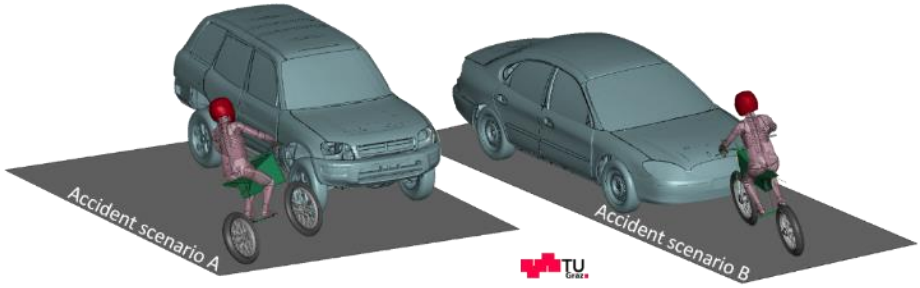

Fig. 7. Setup of the simulation models in the crash scenarios.

Fig. 8 shows the kinematic of the THUMS in Scenario A until ground impact. The THUMS impacted on the right side of the vehicle and impinged frontally with the helmet on the rear lateral window. After a free flight phase, the THUMS hit the ground head first, impacting on the top of the helmet.

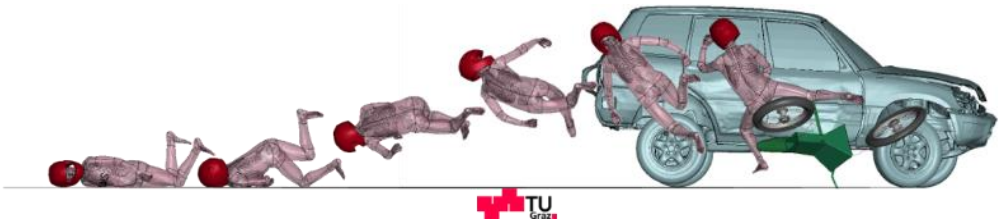

Fig. 8. Kinematics of the moped rider until head impact for crash Scenario A.

The THUMS kinematics from Scenario B are shown in Fig. 10. The THUMS impacted the vehicle frontally at the windscreen, whereby the head impact occurred in the middle of the roof. The THUMS executed a complete rotation to finally impact the ground with the legs first, followed by head impact with the helmet facing sideways.

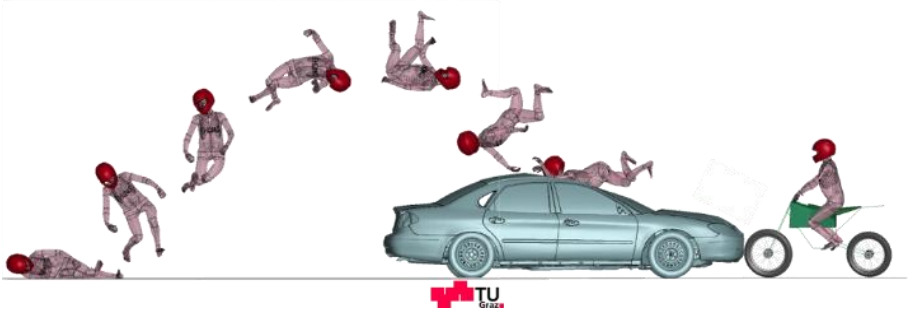

Fig. 10. Kinematics of the moped rider until head impact for crash Scenario B.

Influence of the Helmet Geometry

The parameter study gave insights into the influence of different helmet geometries. Table IV lists the values for CSDM, a3ms, HIC15 , AIS3+ risk for HIC 15, 99th percentile strain of the skull, neck force and neck moment for the simulations with the varied helmet geometries.

It was notable that the CSDM and a3ms values appear low in crash Scenario A, compared to Scenario B. Any risk for AIS3+ head injury was not observed in Scenario A whereas Scenario B showed risk values of up to 16.9%. The 99th percentile strain value of the skull gave no indication for skull fractures in any of the simulation variations. The simulations with the motocross helmet and the motocross helmet with extended chinguard show increased neck forces compared to the corresponding baseline simulation with the full-face helmet. The same situation was seen in the comparison of the neck moments, despite equal values in Scenario B for the simulation with the full-face helmet and the simulation with the motocross helmet.

TABLE IV

INJURY CRITERIA OF DIFFERENT HELMET TYPES

Crash Scenario	Variation	CSDM	a3ms [g]	HIC15 [-]	HIC15 AIS3+ [%]	99th percentile strain – Skull [-]	Neck Force [kN]	Neck Moment [Nm]
A	*Full-face*	0.11	38	70	0	0.002	0.51	49
	Motocross	0.07	32	42	0	0.002	0.61	60
	Motocross chinguard	0.05	37	87	0	0.002	0.67	80
B	*Full-face*	0.38	82	849	16.9	0.003	1.27	56
	Motocross	0.38	85	815	15.6	0.004	1.41	56
	Motocross chinguard	0.40	92	636	8.9	0.003	1.80	118

The evaluation of the calculated injury values in combination with the THUMS kinematics gave further insights into the effects of different helmet geometries. The images in Fig. 9 show the head impact with different helmet types for Scenario A. Comparing the helmet orientations of the full-face and the two motocross helmets revealed an increased rotation of the motocross helmets. As the major rotation occurred about the vertical axis, this value was chosen for comparison. The helmet rotation of the full-face helmet was measured at 17°. An increased

rotation of 25° occurred with both motocross helmets.

The comparison of the calculated injury values supports the negative effects found in the visual evaluation of the head impact. Looking at the neck moment values in Table IV for Scenario A, increased loading was observed for both the motocross helmet and the motocross helmet with extended chinguard.

Full-face Motocross Motocross chinguard

Fig. 9. Head impacts with different helmet types for crash Scenario A.

Fig. 12 depicts the comparison of the full-face helmet, motocross helmet and motocross helmet with extended chinguard for accident Scenario B. The kinematics at head impact show similar trends for the simulations with the full-face helmet and the motocross helmet, although a slightly extended rotation of the motocross helmet was visible. Considering the motocross helmet with the extended chinguard, an obvious relative displacement was noted compared to the full-face helmet. The evaluation of the relative helmet motion was conducted by comparing the rotation about the transverse axis. The baseline simulation with the full-face helmet showed a rotation of 9°, whereas the motocross helmet caused an increased rotation of 36°. However, the simulation with the motocross helmet with extended chinguard showed a further increased rotation of 65°. The injury values in Table IV reveal higher neck force and moment values for the variation involving the extended chinguard.

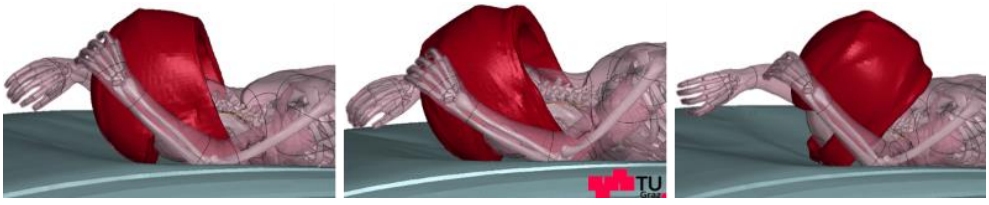

Full-face Motocross Motocross chinguard

Fig. 10. Head impacts with different helmet types for crash Scenario B.

Influence of an Unfastened Chinstrap at Primary Impact

A further parameter variation involved the condition of the chinstrap, in particular keeping the chinstrap fastened and unfastened. For the simulations with the unfastened chinstrap, the chinstrap was removed from the helmet model. TABLE V shows the comparison of the injury criteria from the simulations with the fastened and unfastened chinstrap. Comparing CSDM and a3ms values of the baseline to the modified simulation for both Scenario A and B, no significant difference was noted. Risks for an AIS3+ head injury were noted only in Scenario B. No skull fracture was detected in any simulation when analysing the 99th percentile strain value.

TABLE V
INJURY CRITERIA WITH UNFASTENED CHINSTRAP

Crash Scenario	Variation	CSDM	a3ms [g]	HIC15 [-]	HIC15 AIS3+ [%]	99th percentile strain – Skull [-]	Neck Force [kN]	Neck Moment [Nm]
A	*Full-face*	0.11	38	70	0	0.002	0.51	49
	Full-face without chinstrap	0.19	42	94	0	0.002	0.74	44
B	*Full-face*	0.38	82	849	16.9	0.003	1.27	56
	Full-face without chinstrap	0.50	83	520	5.2	0.006	1.72	95

The head impact involving the unfastened chinstrap from crash Scenario A is shown in Fig. 11. As no visual differences were detected at the moment of head impact, the pictures show the head kinematics 60ms after impacting the car. The helmet began to detach shortly after head impact and led to helmet loss in the subsequent sequences. The comparison of the calculated injury values from Scenario A in Table V merely shows marginal differences, corresponding to the findings in the visual inspection.

A similar behaviour was noted in accident Scenario B. Fig. 12 shows the kinematics 90ms after head impact, where a detachment of the helmet is visible. Table V shows elevated values for neck force and moment.

The simulations with the chinstrap unfastened showed helmet loss immediately after the head impact in both scenarios.

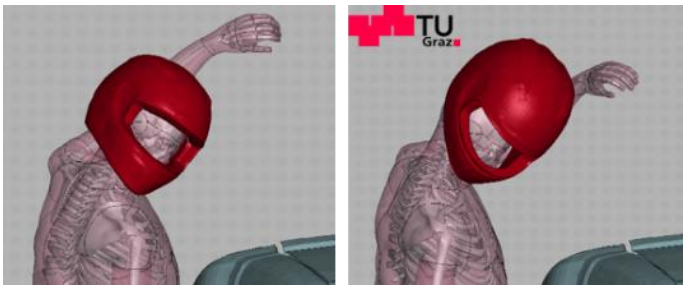

Fig. 11. Head impact with fastened (left) and unfastened (right) chinstrap for crash Scenario A.

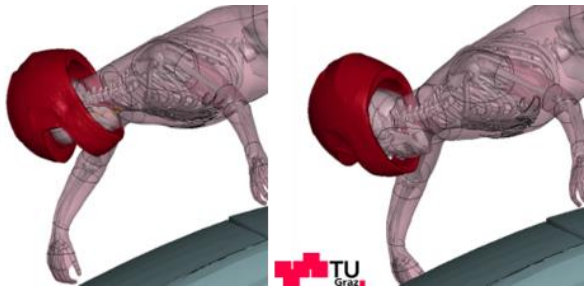

Fig. 12. Head impact with fastened (left) and unfastened (right) chin strap for crash Scenario B.

Evaluation of the Ground Impact

In a further variation step, the ground impact was analysed, through evaluation of the simulation split into two phases. The initial phase, measured from simulation start until 100ms after the head impacting the vehicle, was defined as the primary impact. Phase two, from 100ms after the head impacting the vehicle until the end of the simulation, was defined as the ground impact. The evaluation of each phase was executed separately and the corresponding injury values are listed in TABLE VI.

The ground impact for crash Scenario A shows elevated values for each injury criteria compared to the primary impact, except the CSDM. The unfastened chinstrap simulation showed further elevated injury values, and the HIC value indicated a 64.7% risk for an AIS3+ head injury. The 99th percentile strain value also indicated skull fracture for the unfastened chinstrap simulation by exceeding the threshold of 1.5%.

In Scenario B, elevated values for a3ms and neck moment were noted for the ground impact compared to the primary impact. Increased head loadings were also observed, indicated by an AIS3+ risk of 65.4% for head injuries, whereby the 99th percentile strain value did not diagnose any skull fractures.

TABLE VI
INJURY CRITERIA AT VEHICLE AND GROUND IMPACT

Crash Scenario	Variation	CSDM	a3ms [g]	HIC15 [-]	HIC15 AIS3+ [%]	99th percentile strain – Skull [-]	Neck Force [kN]	Neck Moment [Nm]
A	*Full-face (Primary impact)*	0.11	38	70	0	0.002	0.51	49
	Full-face (Ground impact)	0.03	80	484	4.3	0.003	1.38	62
	Full-face without chinstrap (Ground impact)	0.20	105	2277	64.7	0.055	1.44	125
B	*Full-face (Primary impact)*	0.38	82	849	16.9	0.003	1.27	56
	Full-face (Ground impact)	0.26	169	2314	65.4	0.003	0.89	85

Fig. 15 shows Scenario A kinematics at primary impact, ground impact and ground impact without chinstrap. The head impact conditions differed between the impact to the vehicle and the ground, in that the impact to the vehicle occurred frontally with an overlaid tangential load. In comparison, the THUMS impinged head first to the ground, impacting with the top of the helmet. The simulation without chinstrap showed the same THUMS orientation at ground impact, including the difference of the helmet not being in position to protect the head. Considering the injury values from TABLE VI, the conditions at ground impact led to higher loads on the head and neck compared to the primary impact. Impacting the ground without a fastened chinstrap resulted in even more severe injury values due to the lack of protection of the helmet

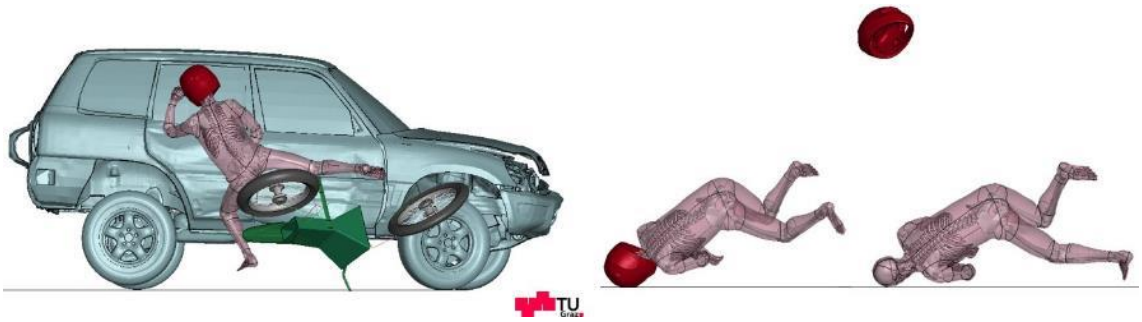

Fig. 15. Kinematics primary impact (left), ground impact (middle) and ground impact without chinstrap (right) for crash Scenario A.

Fig. 13 shows the kinematics at primary impact and ground impact of Scenario B. Also in this scenario, different head impact conditions were observed for the primary and ground impact. As the THUMS hit the roof of the vehicle, chinguard first, the ground impact occurred with the THUMS head facing sideways.

Evaluating the ground impact, increased head and neck loads were observed, see TABLE VI. The values decreased only for the neck force and CSDM. Nevertheless, the ground impact is more severe with regard to the risk of sustaining head injuries.

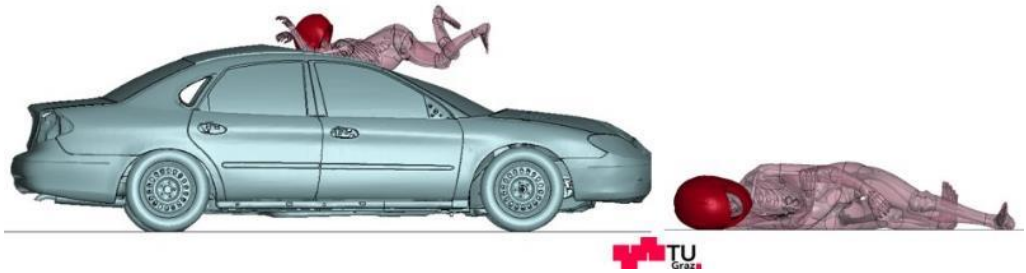

Fig. 13. Kinematics primary impact (left) and ground impact (right) for crash Scenario B.

IV. DISCUSSION

Helmet Modelling

The validation of the helmet models led to adequate results for the purposes of this study. The aim was not to replicate the behaviour of one helmet, rather to design a realistic helmet model suitable for the parameter study. Ultimately, a third of the validation cases achieved a CORA rating above 0.7. Correlation with a CORA rating below 0.5 was found for seven cases, which may result from the test setup and the assumption of a simplified homogenous foam in the FE model. Material parameters were chosen to meet the best average fit over all validation load cases.

It was decided to neglect the comfort foam, as the layer was either too stiff and therefore showed poorer correlation with the tests or the model was numerically instable. Adopting this particular modelling approach, without comfort foam, led to adequate kinematic behaviour and has already been applied in other studies [26].

The helmet impact speed for the drop tests was defined based on standard drop test procedures. Fall height limitations at the utilised test bench made tests above a speed of 27 km/h unsuitable. Differences in head impact velocities were exposed during the comparison of the simulated accident scenarios. Table V lists the head impact velocity at primary impact as well as the impact velocity at the ground of both accident scenarios. The ground

impact velocities of the scenarios roughly meet the dimensions of the drop test velocities from standardised test procedures. A distinct higher value was noted when looking at the primary impact velocity of Scenario B. The vehicle velocity in this scenario adds up to the head velocity of the THMUS, leading to a higher impact velocity.

Considering these findings in the light of the fact that the standard for testing helmets is at a velocity of 27km/h, highlights the need for enhancing standard helmet test procedures, which is in line with other studies as well [27].

TABLE V
HEAD IMPACT VELOCITIES OF THE SIMULATED REAL-WORLD ACCIDENTS

	Head Impact velocity at vehicle [km/h]	Head Impact velocity on ground [km/h]
Scenario A	14	22
Scenario B	75	34

Application of THUMS v4 for Simulation of Real-World Accidents

THUMS v4 was used in previous studies to replicate injuries to Post-Mortem Human Subject (PMHS) tests and real-world accidents with regard to car occupants, pedestrians and cyclists [4–11]. Although moped and motorcycle riders account for 10.3% of the road fatalities worldwide [28], this study is the first to apply the THUMS v4 for the evaluation of injuries sustained by moped riders. The study serves as an initial trial to evaluate if HBM simulations will lead to meaningful results for the high relative speeds reached by moped riders in comparison to pedestrian and cyclists, the low level of protection, especially in relation to vehicle occupants, as well as the lack of validation data.

As the setup of the simulations were replicated based on the information specified in the technical reports, detailed validation of the kinematics, head impact points and injuries was not conducted. The accident reconstructions itself, (i.e., simulating several variations until ground impact to identify boundary conditions leading to the final positions and traces described in the police reports), were not performed with THUMS due to long simulation times required. Although accident reconstructions by the software PC Crash (multibody simulation) [29] were available, they were not used for the validation. The kinematics of the multibody model is an approximation and therefore give no further information about the behaviour of moped riders in real-world crashes.

Information about the injuries sustained by the moped rider in Scenario A was provided through a medical report, which was compared to the injuries diagnosed with the THUMS in the corresponding simulation. Brain and organ injuries as well as skull fractures were reproduced in the accident simulation, however rib, pelvis and femur fractures could not be diagnosed. The quality of injury reproduction would be boosted with access to knowledge about exact impact conditions and moped rider behaviour. Deviation to the parameters would result in different loadings on the moped rider and would influence the injury outcome. Further, it is unclear if or how the moped riders reacted prior to impact and during the flight phase, which might also affect kinematics and injury outcome. The accident simulations represent approximations of actual real-world crashes. Nevertheless, a relative comparison of injury values when varying the helmet parameters provides valuable insights as to any contributing influencing factors involved.

The study shows that the results from the HBM simulations are plausible. However, the next step required would be to generate further validated model-specific probabilistic injury criteria, to facilitate research and safety engineers in performing reliable injury risk assessments of injury for the relevant body regions.

No validated strain-based assessment criteria are available for the THUMS v4 skull. Hence, the current study has applied thresholds and criteria used in previous studies [24-25]. However, it is remarkable that trends for the strain-based skull fracture predictions and the HIC values are different in some of the cases. Based on [22], HIC seems to be a reliable predictor for skull fracture for the THUMS v4.02.

Furthermore, to gain a clearer picture, simulation of a higher number of real-world cases would be required. Generally, the results found in this study are based on the variation of helmet parameters from two different load scenarios. Despite the load cases producing different head impact conditions, the results of the investigation are restricted to those particular scenarios. If extending the evaluation to further load cases, additional findings may be derived.

Effect of Different Helmet Types and Chinstrap

In a comparison of the different helmet geometries, the protruding chinguard facilitated rotation of the helmet. As the movement between head and helmet was simply restricted by the chinstrap and the defined contact, a relative deflection was visible in the simulation results. The applied modelling method can, therefore, be seen as a worst-case scenario in terms of helmet fit due to the exclusion of the comfort foam. Nevertheless, increasing neck loadings were measured in the simulations with extended chinguard geometry. Despite the relative displacement of the helmet, the movement of the helmet still induced the head to rotate.

Assuming a tight fit of the helmet, neck loadings could further increase, if the entire rotation is transferred by the helmet. Hence, in order to support this thesis, a helmet model with a validated comfort foam layer is required.

Both simulation variations with the chinstrap unfastened led to loss of the helmet. The helmet detached due to the force active while impacting the vehicle. Once again, the worst-case scenario, involving loose fit of the helmet must be highlighted. Nevertheless, the simulation models fulfilled the purpose of revealing possible risks arising from misuse conditions. The analysis of the influence of fitting conditions on helmet loss would be a task for further investigations.

Comparison of Primary and Ground Impact

When looking at the AIS3+ risk values from the primary and ground impact phases in accident Scenario A, only a minor risk of head injury is noticeable in the ground impact, due to the helmet fitting well over the entire accident duration. Furthermore, the skull strain values gave no indication of skull fracture. Nevertheless, increased neck loadings were documented in the ground impact compared to the primary impact. Due to the orientation of the THUMS, the head of the motorcyclist impacted the ground first, followed by the rest of the body causing high loadings to the neck. For the same reason, a high head acceleration value was noted.

In crash Scenario B, neck forces and CSDM values decreased in the ground impact. The higher neck-force at the primary impact was assumed to result from the impact on the chinguard generating tension and shear loadings on the neck. The neck force for the ground impact was lower, as a sheer translational impact on the side of the head occurred. This translational impact led to a significantly increased head acceleration, which is also notable in a high risk of 65.4% for an AIS3+ head injury. Despite such high HIC-based risk, no critical head loading was prognosticated by the strain value of the skull.

Increased injury values were detected when comparing the simulation of the ground impact with and without chinstrap for Scenario A. When no head protection was present due to helmet loss, head acceleration and the risk of skull fracture on ground impact increased drastically. The ground impact without chinstrap of Scenario B could not be simulated due to instabilities of the model. Nevertheless, increased head loads measured in the simulation without chinstrap highlight the head protection potential of the helmet.

V. CONCLUSIONS

The simulations of crash scenarios based on real-world moped accidents with THUMS v4 carried out in this study led to plausible results. The comparison of two different helmet shapes revealed a negative effect of the protruding chinguard of the motocross helmet in the analysed real-world conditions. In impacts, the lever effect on this particular protruding part led to high neck loadings due to rotation of the helmet. Simulation variations with unfastened chinstraps led to helmet loss after the primary impact. The subsequent unprotected head impact to the ground revealed high injury risks. However, current isolated helmet tests do not support evaluation of these effects. Hence, the current study highlights the importance of applying real-world loading conditions in future investigations.

VI. ACKNOWLEDGEMENT

The authors would like to thank the Austrian Ministry for Climate Protection, Environment, Energy, Transport, Innovation and Technology (bmk) for funding the study via the Austrian Traffic Safety Fond (VSF). The authors are grateful to the Austrian Automobile Club (ÖAMTC) and the Research Center for Infantile Accidents at the University Hospital in Graz for the collaboration in this study. Further, we would like to acknowledge the use of High Performance Cluster resources provided by the ZID (IT services) at Graz University of Technology, Austria.

VII. REFERENCES

1. Statistik Austria. (2019) *Straßenverkehrsunfälle Jahresergebnisse 2018*, Wien, Austria.
2. ACEM. (2009) *Motorcycle Accident in Depth Study (MAIDS) - In-Depth investigations of accidents involving powered two wheelers*, Brussels, Belgium.
3. Vehicle Safety Institute. "CEDATU", https://www.tugraz.at/institute/vsi/unfalldatenbank-zedatu/allgemeine-informationen/ [Accessed 15 June 2018].
4. Klug C, Feist F, Wimmer P. (2018) Simulation of a Selected Real World Car to Bicyclist Accident using a Detailed Human Body Model. *Proceedings of IRCOBI Conference,* 2018, Athens, Greece.
5. Fahlstedt M, Halldin P, Alvarez VS, Kleiven S. (2016) Influence of the Body and Neck on Head Kinematics and Brain Injury Risk in Bicycle Accident Situations. *Proceedings of IRCOBI Conference,* 2016, Malaga, Spain.
6. Fahlstedt M, Halldin P, Kleiven S. (2016) Comparison of Multibody and Finite Element Human Body Models in Pedestrian Accidents with the Focus on Head Kinematics. *Traffic Injury Prevention, **17**(3)*: pp.320–327.
7. Ghosh P, Mayer C, Deck C, Bourdet N, Meyer F, Willinger R, et al. *(*2016) Head Injury Risk Assessment in Pedestrian Impacts on Small Electric Vehicles using Coupled SUFEHM-THUMS Human Body Models Running in Different Crash Codes. *Proceedings of IRCOBI Conference,* 2016, Malaga, Spain.
8. Coulongeat F, Roth F, Schenk T, Seibert D. (2014) Simulation of a Real Accident with a Pedestrian using a FE Human Model: Potential from the View of Integrated Safety. *Proceedings of IRCOBI Conference,* 2014, Berlin, Germany.
9. Iwamoto M, Nakahira Y. (2014) A Preliminary Study to Investigate Muscular Effects for Pedestrian Kinematics and Injuries Using Active THUMS. *Proceedings of IRCOBI Conference,* 2014, Berlin, Germany.
10. Pal C, Okabe T, Vimalathithan K, Manoharan J, Muthanandam M, Narayanan S. (2014) Estimation of Pelvis Injuries and Head Impact Time using Different Pedestrian Human FE Models. *Proceedings of SAE 2014 World Congress & Exhibition,* 2014.
11. Bastien C, Orlowski M, Bhagwani M. (2017) Validation of Finite Element Human Model Throw Distance in Pedestrian Accident Scenarios. *Proceedings of 11th European LS-DYNA Conference, 2017,* Coventry, United Kingdom.
12. Huang Y, Zhou Q, Tang J, Nie B. (2018) A Preliminary Comparative Study on Rider Kinematics and Injury Mechanism in Car-to-two-wheelers Collision. *Proceedings of IRCOBI Conference,* 2018, Athens, Greece.
13. Sun J, Rojas A, Kraenzler R, Arnoux PJ. (2012) Investigation of Motorcyclist Safety Systems Contributions to Prevent Cervical Spine Injuries using HUMOS Model. *International Journal of Crashworthiness, **17**(6)*: pp.571–581.
14. Klug C, Feist F, Tomasch E. (2015) CLEVERER HELM - Optimaler Schutz vor Kopfverletzungen durch verbesserte Testmethoden von Kinder-Fahrradhelmen, *Austrian Ministry for Climate Protection, Environment, Energy, Transport, Innovation and Technology*, Wien, Austria.
15. Kitagawa Y, Yasuki T. (2014) Development and Application of THUMS Version 4. *Proceedings of 5th International Symposium: Human Modelling and Simulation in Automotive Engineering,* 2014, Munich, Germany.
16. Iraeus J, Lindquist M. (2016) Development and Validation of a Generic Finite Element Vehicle Buck Model for the Analysis of Driver Rib Fractures in Real Life Nearside Oblique Frontal Crashes. *Accident Analysis & Prevention, 95*: pp. 42–56.
17. UNECE. (2002) A*ddendum21: Regulation No 22 Uniform Provisions Concerning the Approval of Protective Helmets and their Visor for Drivers and Passengers of Motor Cycle and Mopeds*.
18. ESI Group. (2014) *Virtual Performance Solution 2014*, Paris, France.
19. The George Washington University, Washington D.C., https://www.nhtsa.gov/crash-simulation-vehicle-models [Accessed 6 September 2018].
20. Watanabe R, Miyazaki H, Kitagawa Y, Yasuki T. (2011) Research of the Relationship of Pedestrian Injury to Collision Speed, Car-type, Impact Location and Pedestrian Sizes Using Human FE Model (THUMS Version 4). *Proceedings of International Technical Conference on the Enhanced Safety of Vehicles,* 2011, Washington, D.C., USA.
21. Miller L, Gaewsky J, Weaver A, Stitzel J, White N. (2016) Regional Level Crash Induced Injury Metrics Implemented within THUMS v4.01, 2016, *Proceedings of SAE 2016 World Congress & Exhibition,* 2016.
22. Liangliang Shi, Yong Han, Hongwu Huang, Johan Davidsson, Robert Thomson (2020) Evaluation of Injury

Thresholds for Predicting Severe Head Injuries in Vulnerable Road Users resulting from Ground Impact via Detailed Accident Reconstructions. *Biomechanics and Modelling in Mechanobiology 2020*: pp.1–19.
23. Kuppa S. (2004) Injury Criteria for Side Impact Dummies. *National Highway Traffic Safety Administration, 2004*: pp 1-68.
24. Wu T, Kim T, Bollapragada V, Poulard D, Chen H, Panzer MB, *et al.* (2017) Evaluation of Biofidelity of THUMS Pedestrian Model under a Whole-body Impact Conditions with a Generic Sedan Buck. *Traffic Injury Prevention*, Washington D.C, US.
25. Chen H, Poulard D, Forman J, Crandall J, Panzer MB. (2018) Evaluation of Geometrically Personalized THUMS Pedestrian Model Response against Sedan-pedestrian PMHS Impact Test Data. *Traffic Injury Prevention 2018*: pp.1–7.
26. Ghajari M, Peldschus S, Galvanetto U, Iannucci L. (2013) Effects of the Presence of the Body in Helmet Oblique Impacts. *Accident Analysis & Prevention*, **50**: pp. 263–271.
27. Bourdet N, Mojumder S, Piantini S, Deck C, Pierini M, Willinger R. (2016) Proposal of a New Motorcycle Helmet Test Method for Tangential Impact. *Proceedings of IRCOBI Conference,* 2016, Malaga, Spain.
28. Bakker J. (2012) iGLAD - Ein Pragmatischer Ansatz für eine Internationale Unfalldatenbank. In: VDA Verband der Automobilindustrie e. V. (ed). *14th VDA Technical Congress*, 2014, Sindelfingen, Germany.
29. DSD. (2014) *PC-Crash: Ein Simulationsprogramm für Verkehrsunfälle. Bedienungs- und technisches Handbuch*, Linz, Austria.

VIII. APPENDIX

Fig. A1: Comparison of the kinematics: Full-face helmet – frontal – 0° anvil.

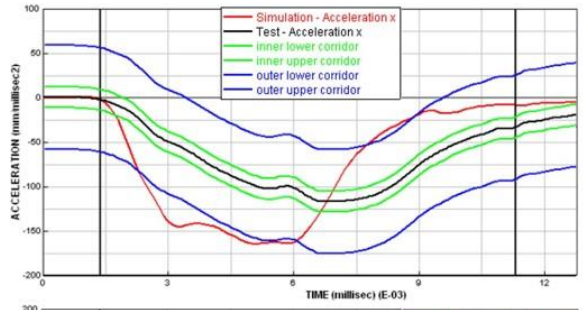

No.	Name				Rating	Weight
1	Corridor Method				0.1899	0.5
2	Correlation method	Value	Rating	Weight	0.4269	0.5
a	Cross correlation function	0.9731	0.9602	0.2		
b	Size	0.5872	0.5872	0.4		
c	Phase shift	0.0018	0.0	0.4		
3	Combination of 1 and 2				0.3084	
	Overall Rating:	**0.3084**				

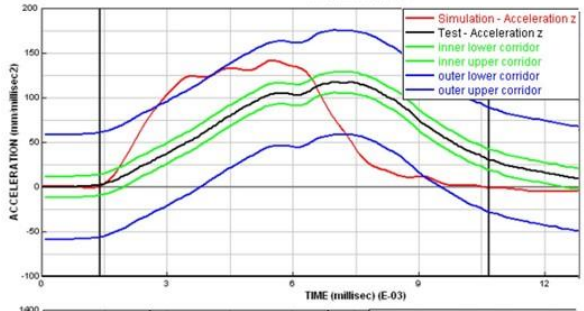

No.	Name				Rating	Weight
1	Corridor Method				0.2001	0.5
2	Correlation method	Value	Rating	Weight	0.5192	0.5
a	Cross correlation function	0.9718	0.9583	0.2		
b	Size	0.8188	0.8188	0.4		
c	Phase shift	0.0018	0.0	0.4		
3	Combination of 1 and 2				0.3596	
	Overall Rating:	**0.3596**				

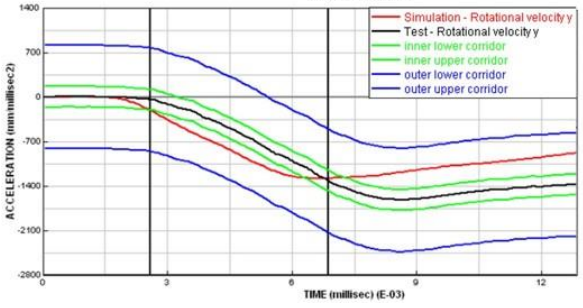

No.	Name				Rating	Weight
1	Corridor Method				0.6955	0.5
2	Correlation method	Value	Rating	Weight	0.5833	0.5
a	Cross correlation function	0.9951	0.9927	0.2		
b	Size	0.9618	0.9618	0.4		
c	Phase shift	0.0008	0.0	0.4		
3	Combination of 1 and 2				0.6394	
	Overall Rating:	**0.6394**				

Fig. A2: CORA ratings of the acceleration and rotational velocity curves: Full-face helmet – frontal – 0° anvil.

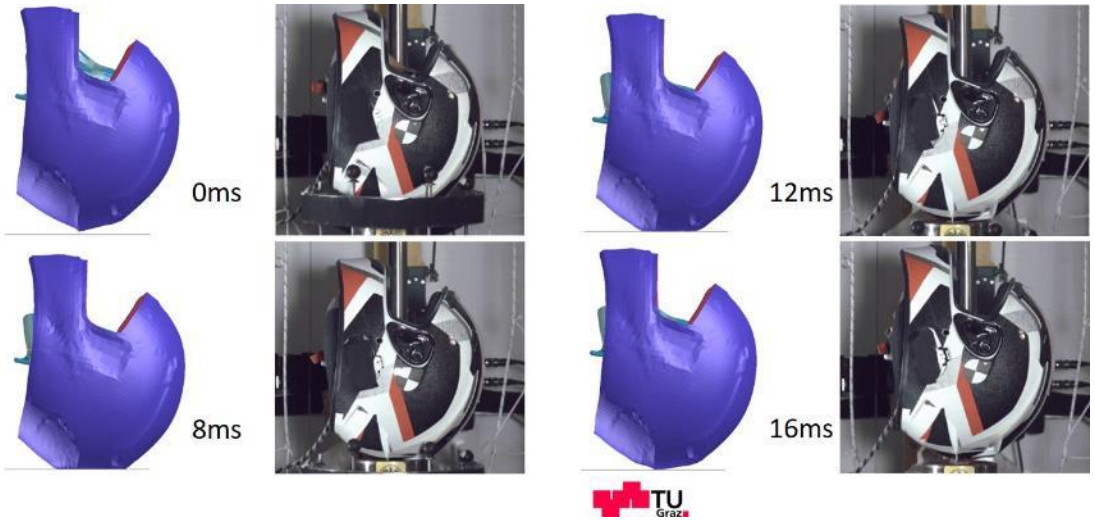

Fig. A3. Comparison of the kinematics: full-face helmet – rear – 0° anvil.

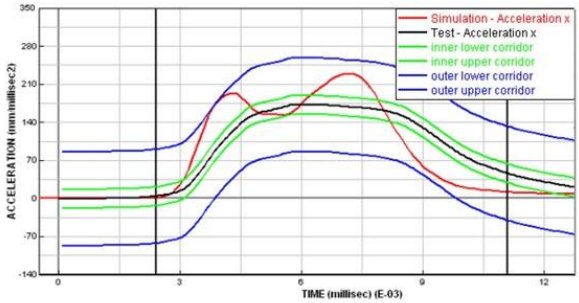

No.	Name				Rating	Weight
1	Corridor Method				0.4903	0.5
2	Correlation method	Value	Rating	Weight	0.6978	0.5
a	Cross correlation function	0.9728	0.9598	0.2		
b	Size	0.8357	0.8357	0.4		
c	Phase shift	0.0007	0.4289	0.4		
3	Combination of 1 and 2				0.594	
	Overall Rating:	**0.594**				

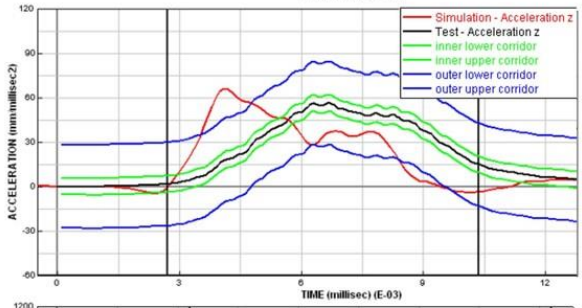

No.	Name				Rating	Weight
1	Corridor Method				0.2422	0.5
2	Correlation method	Value	Rating	Weight	0.5521	0.5
a	Cross correlation function	0.9571	0.937	0.2		
b	Size	0.9118	0.9118	0.4		
c	Phase shift	0.0015	0.0	0.4		
3	Combination of 1 and 2				0.3971	
	Overall Rating:	**0.3971**				

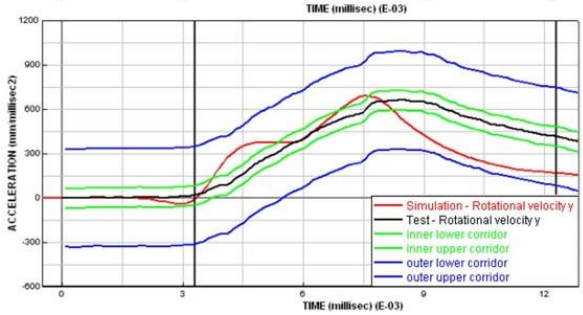

No.	Name				Rating	Weight
1	Corridor Method				0.514	0.5
2	Correlation method	Value	Rating	Weight	0.4595	0.5
a	Cross correlation function	0.9745	0.9622	0.2		
b	Size	0.6677	0.6677	0.4		
c	Phase shift	0.0012	0.0	0.4		
3	Combination of 1 and 2				0.4868	
	Overall Rating:	**0.4868**				

Fig. A4. CORA ratings of the acceleration and rotational velocity curves: full-face helmet – rear – 0° anvil.

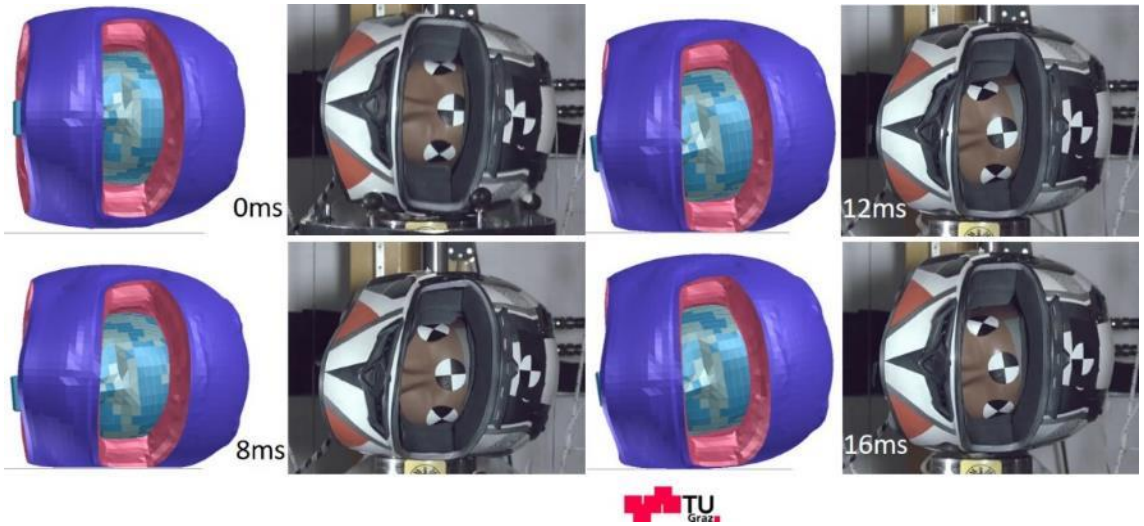

Fig. A5. Comparison of the kinematics: full-face helmet – side – 0° anvil.

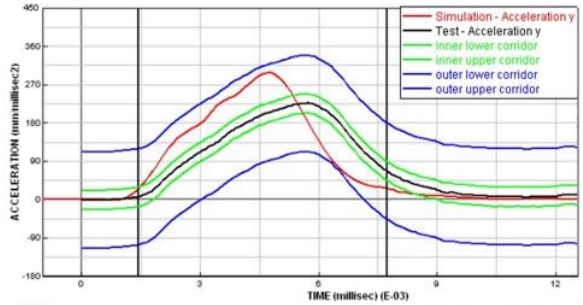

No.	Name				Rating	Weight
1	Corridor Method				0.2897	0.5
2	Correlation method	Value	Rating	Weight	0.4916	0.5
a	Cross correlation function	0.9918	0.9878	0.2		
b	Size	0.735	0.735	0.4		
c	Phase shift	0.0009	0.0	0.4		
3	Combination of 1 and 2				0.3907	
	Overall Rating:	**0.3907**				

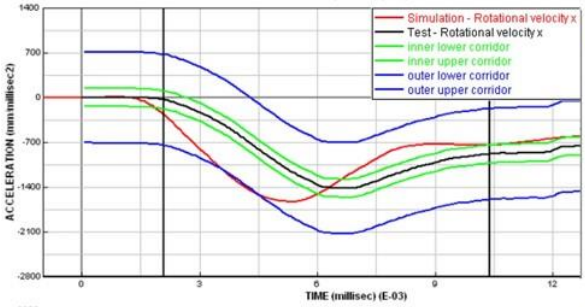

No.	Name				Rating	Weight
1	Corridor Method				0.4323	0.5
2	Correlation method	Value	Rating	Weight	0.5641	0.5
a	Cross correlation function	0.9929	0.9894	0.2		
b	Size	0.9157	0.9157	0.4		
c	Phase shift	0.0013	0.0	0.4		
3	Combination of 1 and 2				0.4982	
	Overall Rating:	**0.4982**				

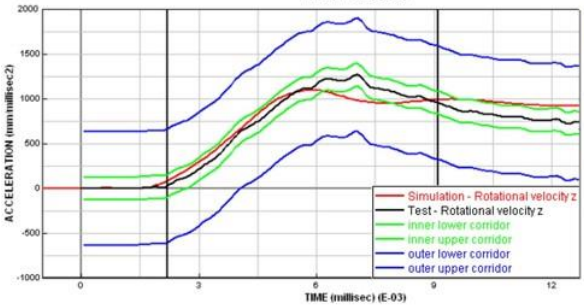

No.	Name				Rating	Weight
1	Corridor Method				0.9474	0.5
2	Correlation method	Value	Rating	Weight	0.806	0.5
a	Cross correlation function	0.9979	0.9968	0.2		
b	Size	0.8369	0.8369	0.4		
c	Phase shift	0.0004	0.6797	0.4		
3	Combination of 1 and 2				0.8767	
	Overall Rating:	**0.8767**				

Fig. A6. CORA ratings of the acceleration and rotational velocity curves: full-face helmet – side – 0° anvil.

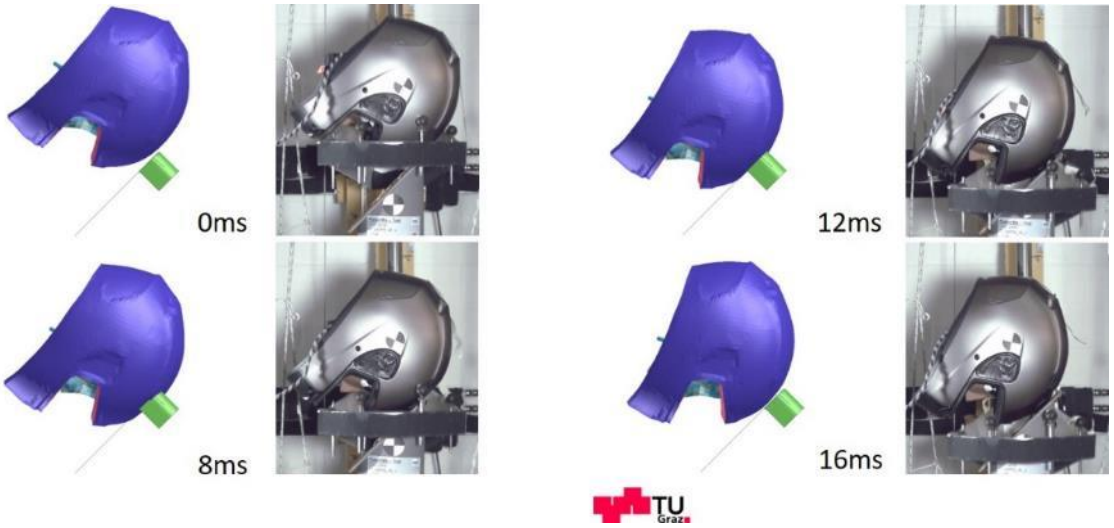

Fig. A7. Comparison of the kinematics: full-face helmet – frontal – 45° anvil.

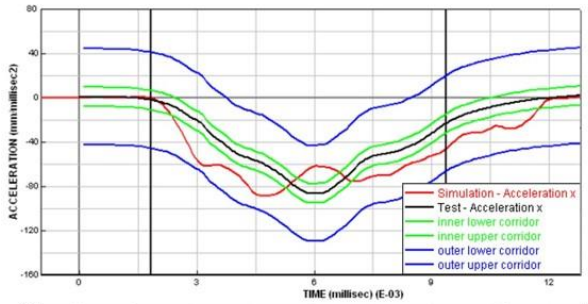

No.	Name				Rating	Weight
1	Corridor Method				0.5269	0.5
2	Correlation method	Value	Rating	Weight	0.7674	0.5
a	Cross correlation function	0.9643	0.9474	0.2		
b	Size	0.7121	0.7121	0.4		
c	Phase shift	0.0004	0.7327	0.4		
3	Combination of 1 and 2				0.6472	
	Overall Rating:	**0.6472**				

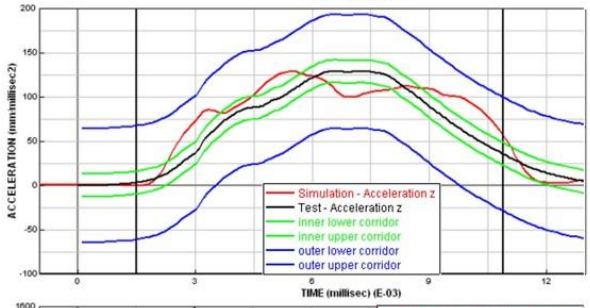

No.	Name				Rating	Weight
1	Corridor Method				0.716	0.5
2	Correlation method	Value	Rating	Weight	0.9366	0.5
a	Cross correlation function	0.9745	0.9623	0.2		
b	Size	0.8603	0.8603	0.4		
c	Phase shift	0.0001	1.0	0.4		
3	Combination of 1 and 2				0.8263	
	Overall Rating:	**0.8263**				

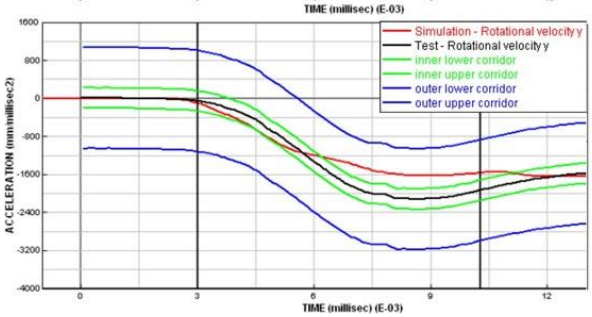

No.	Name				Rating	Weight
1	Corridor Method				0.737	0.5
2	Correlation method	Value	Rating	Weight	0.5994	0.5
a	Cross correlation function	0.9972	0.9957	0.2		
b	Size	0.5933	0.5933	0.4		
c	Phase shift	0.0006	0.4074	0.4		
3	Combination of 1 and 2				0.6682	
	Overall Rating:	**0.6682**				

Fig. A8. CORA ratings of the acceleration and rotational velocity curves: full-face helmet – frontal – 45° anvil

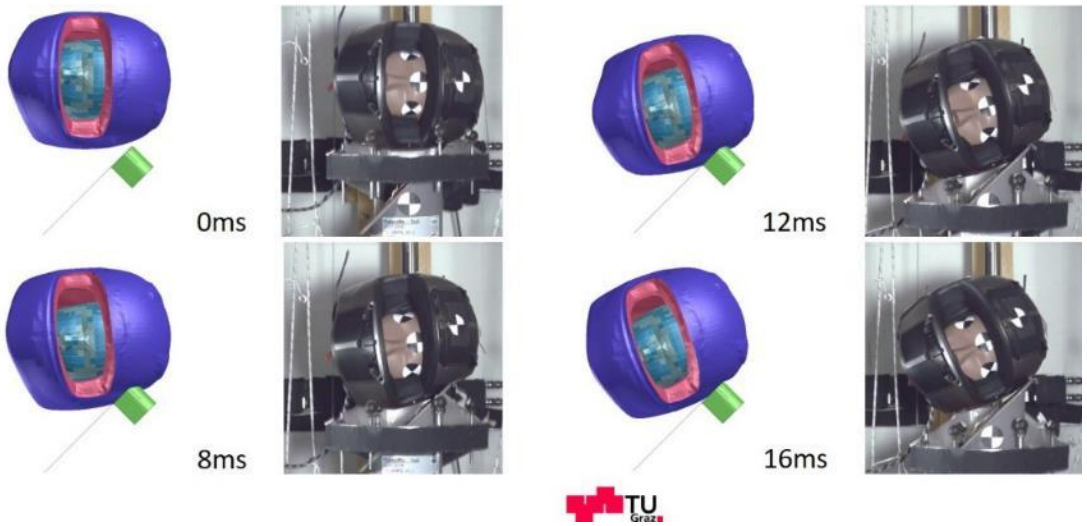

Fig. A9. Comparison of the kinematics: full-face helmet – side – 45° anvil.

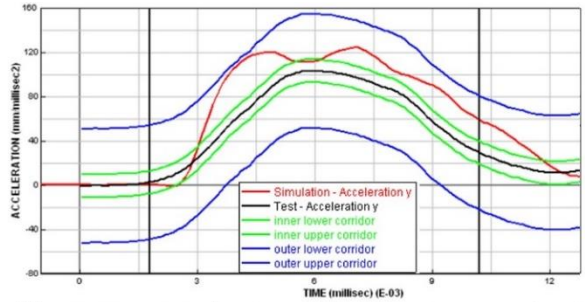

No.	Name				Rating	Weight
1	Corridor Method				0.5045	0.5
2	Correlation method	Value	Rating	Weight	0.8257	0.5
a	Cross correlation function	0.9861	0.9794	0.2		
b	Size	0.5746	0.5746	0.4		
c	Phase shift	0.0001	1.0	0.4		
3	Combination of 1 and 2				0.6651	
	Overall Rating:	**0.6651**				

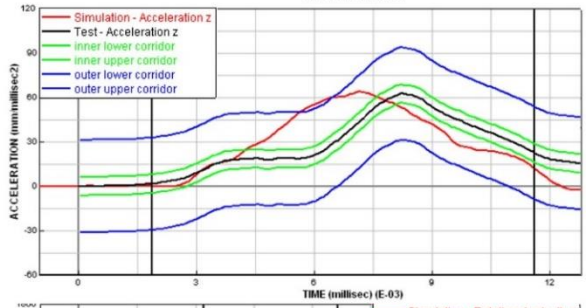

No.	Name				Rating	Weight
1	Corridor Method				0.5902	0.5
2	Correlation method	Value	Rating	Weight	0.5333	0.5
a	Cross correlation function	0.9837	0.9757	0.2		
b	Size	0.8454	0.8454	0.4		
c	Phase shift	0.0014	0.0	0.4		
3	Combination of 1 and 2				0.5617	
	Overall Rating:	**0.5617**				

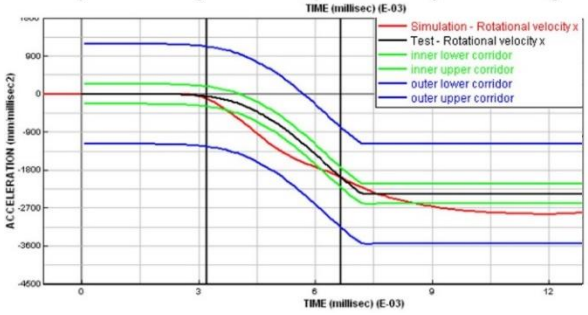

No.	Name				Rating	Weight
1	Corridor Method				0.7284	0.5
2	Correlation method	Value	Rating	Weight	0.589	0.5
a	Cross correlation function	0.9915	0.9873	0.2		
b	Size	0.979	0.979	0.4		
c	Phase shift	0.0006	0.0	0.4		
3	Combination of 1 and 2				0.6587	
	Overall Rating:	**0.6587**				

Fig. A10. CORA ratings of the acceleration and rotational velocity curves: full-face helmet – side – 45° anvil

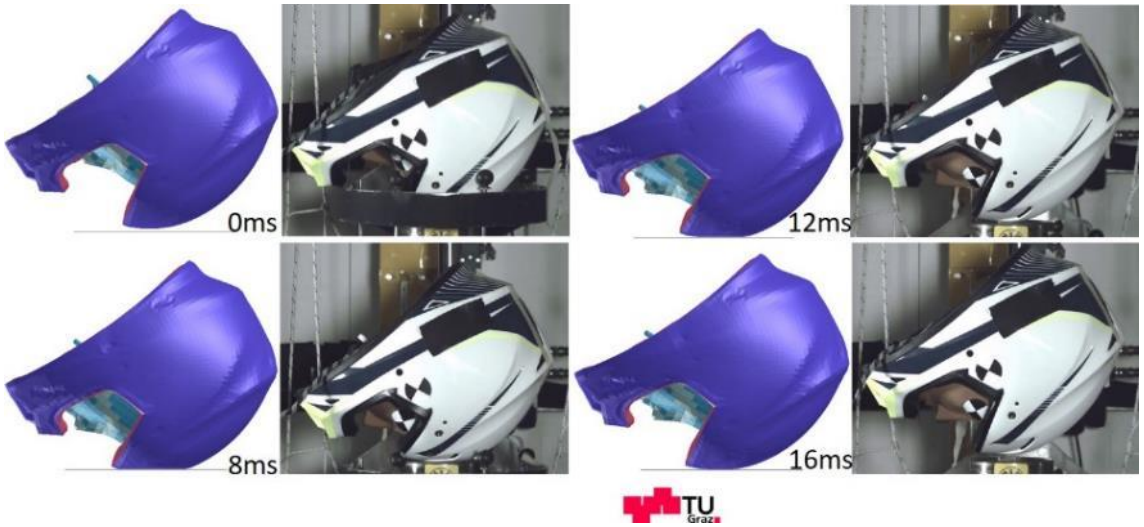

Fig. A11. Comparison of the kinematics: motocross helmet – frontal – 0° anvil.

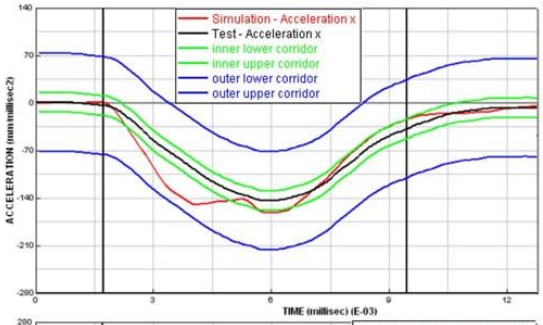

No.	Name				Rating	Weight
1	Corridor Method				0.7838	0.5
2	Correlation method	Value	Rating	Weight	0.7428	0.5
a	Cross correlation function	0.9947	0.9921	0.2		
b	Size	0.7587	0.7587	0.4		
c	Phase shift	0.0005	0.6023	0.4		
3	Combination of 1 and 2				0.7633	
	Overall Rating:	**0.7633**				

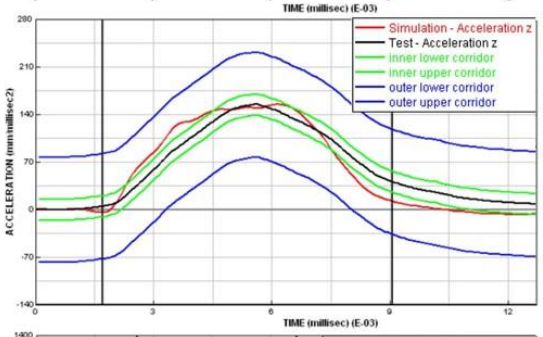

No.	Name				Rating	Weight
1	Corridor Method				0.8458	0.5
2	Correlation method	Value	Rating	Weight	0.9065	0.5
a	Cross correlation function	0.9932	0.9899	0.2		
b	Size	0.901	0.901	0.4		
c	Phase shift	0.0003	0.8704	0.4		
3	Combination of 1 and 2				0.8761	
	Overall Rating:	**0.8761**				

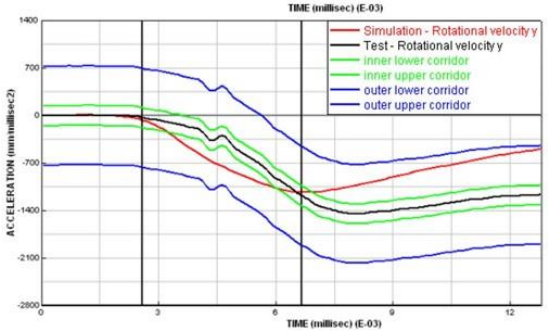

No.	Name				Rating	Weight
1	Corridor Method				0.6992	0.5
2	Correlation method	Value	Rating	Weight	0.5751	0.5
a	Cross correlation function	0.9873	0.981	0.2		
b	Size	0.9472	0.9472	0.4		
c	Phase shift	0.0007	0.0	0.4		
3	Combination of 1 and 2				0.6371	
	Overall Rating:	**0.6371**				

Fig. A12. CORA ratings of the acceleration and rotational velocity curves: motocross helmet – frontal – 0° anvil.

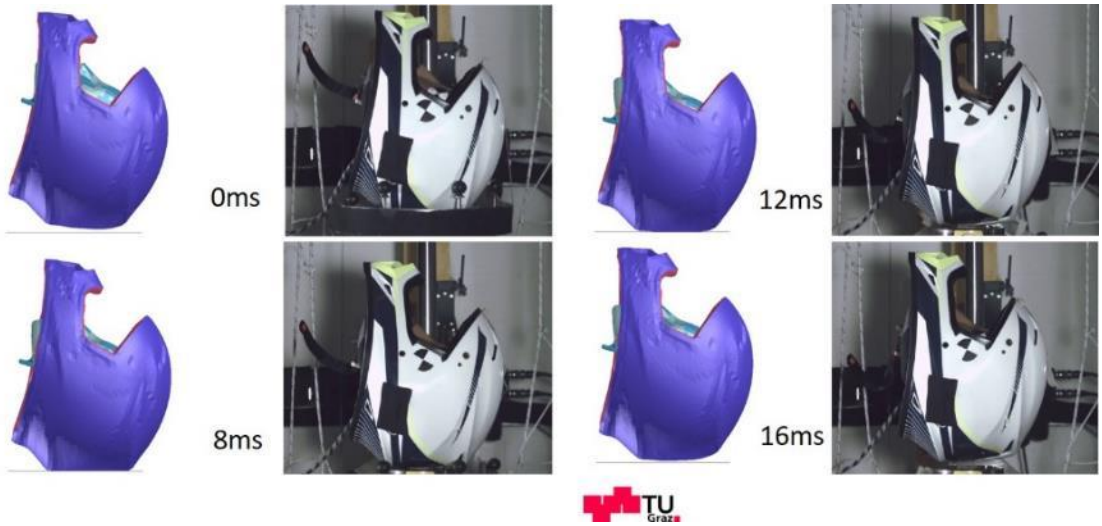

Fig. A13. Comparison of the kinematics: motocross helmet – rear – 0° anvil.

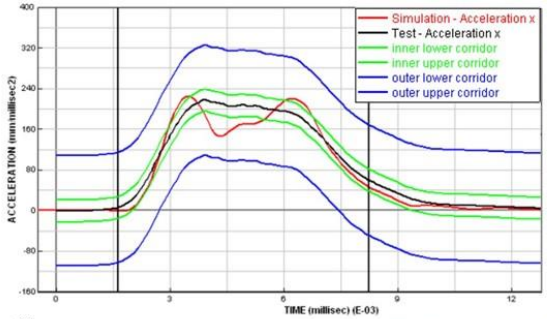

No.	Name				Rating	Weight
1	Corridor Method				0.8697	0.5
2	Correlation method	Value	Rating	Weight	0.9669	0.5
a	Cross correlation function	0.9858	0.9789	0.2		
b	Size	0.9278	0.9278	0.4		
c	Phase shift	0.0	1.0	0.4		
3	Combination of 1 and 2				0.9183	
	Overall Rating:	**0.9183**				

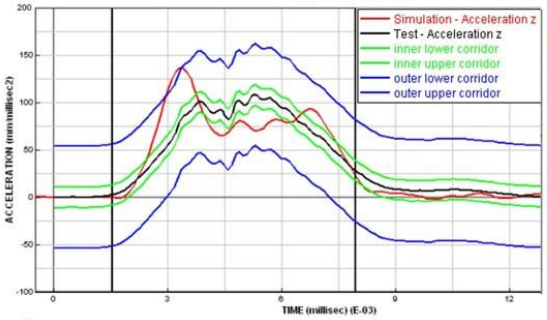

No.	Name				Rating	Weight
1	Corridor Method				0.6447	0.5
2	Correlation method	Value	Rating	Weight	0.8719	0.5
a	Cross correlation function	0.9548	0.9337	0.2		
b	Size	0.9086	0.9086	0.4		
c	Phase shift	0.0003	0.8042	0.4		
3	Combination of 1 and 2				0.7583	
	Overall Rating:	**0.7583**				

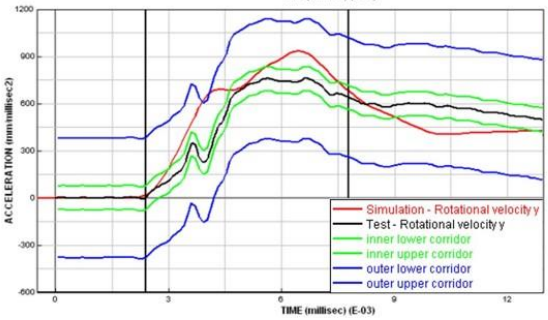

No.	Name				Rating	Weight
1	Corridor Method				0.6811	0.5
2	Correlation method	Value	Rating	Weight	0.6924	0.5
a	Cross correlation function	0.9913	0.987	0.2		
b	Size	0.7429	0.7429	0.4		
c	Phase shift	0.0004	0.4948	0.4		
3	Combination of 1 and 2				0.6868	
	Overall Rating:	**0.6868**				

Fig. A14. CORA ratings of the acceleration and rotational velocity curves: motocross helmet – rear – 0° anvil.

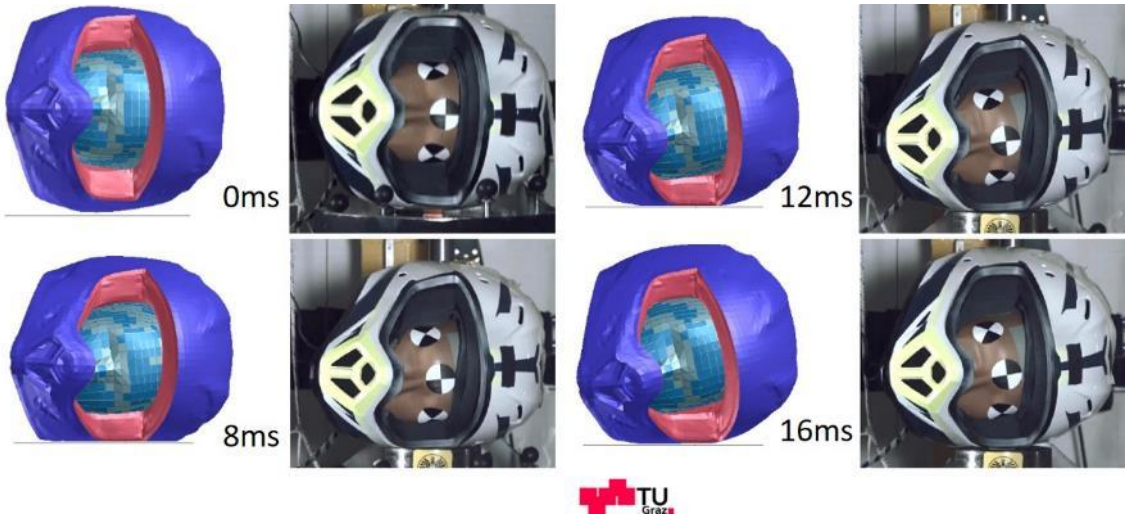

Fig. A15. Comparison of the kinematics: motocross helmet – side – 0° anvil.

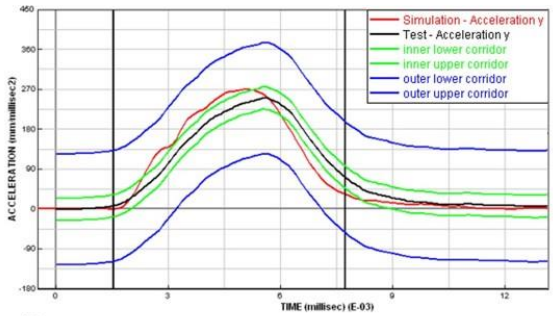

No.	Name				Rating	Weight
1	Corridor Method				0.772	0.5
2	Correlation method	Value	Rating	Weight	0.8	0.5
a	Cross correlation function	0.9965	0.9948	0.2		
b	Size	0.8977	0.8977	0.4		
c	Phase shift	0.0004	0.6047	0.4		
3	Combination of 1 and 2				0.786	
	Overall Rating:	**0.786**				

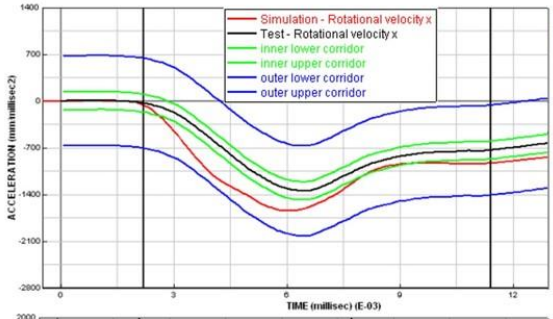

No.	Name				Rating	Weight
1	Corridor Method				0.6403	0.5
2	Correlation method	Value	Rating	Weight	0.7915	0.5
a	Cross correlation function	0.9991	0.9986	0.2		
b	Size	0.6346	0.6346	0.4		
c	Phase shift	0.0004	0.8449	0.4		
3	Combination of 1 and 2				0.7159	
	Overall Rating:	**0.7159**				

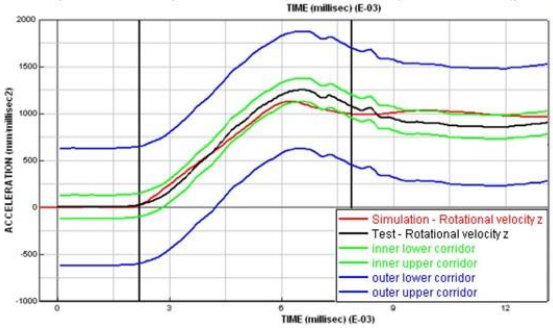

No.	Name				Rating	Weight
1	Corridor Method				0.9845	0.5
2	Correlation method	Value	Rating	Weight	0.9165	0.5
a	Cross correlation function	0.9995	0.9992	0.2		
b	Size	0.7916	0.7916	0.4		
c	Phase shift	0.0001	1.0	0.4		
3	Combination of 1 and 2				0.9505	
	Overall Rating:	**0.9505**				

Fig. A16. CORA ratings of the acceleration and rotational velocity curves: motocross helmet – side – 0° anvil.

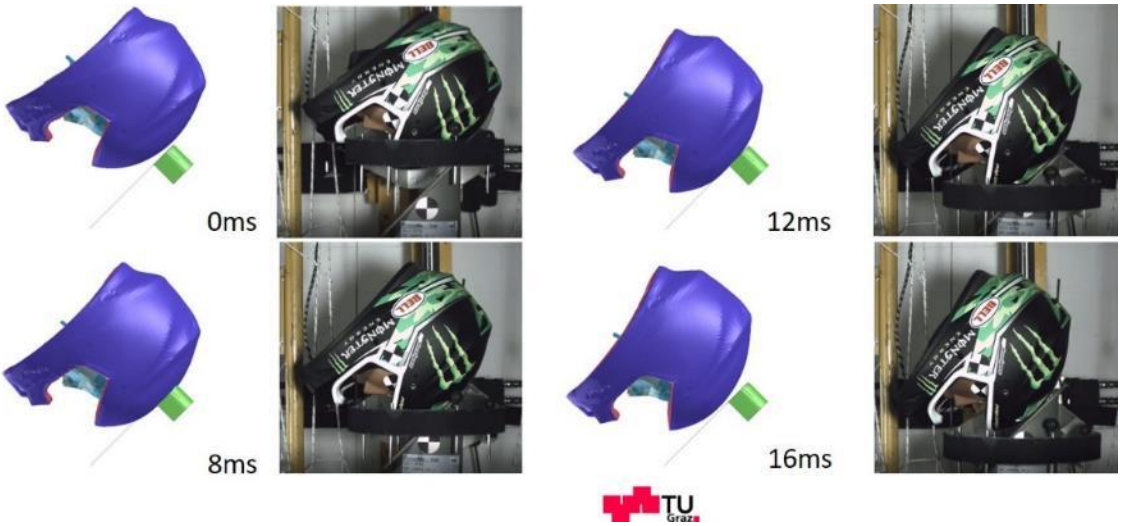

Fig. A17. Comparison of the kinematics: motocross helmet – frontal – 45° anvil.

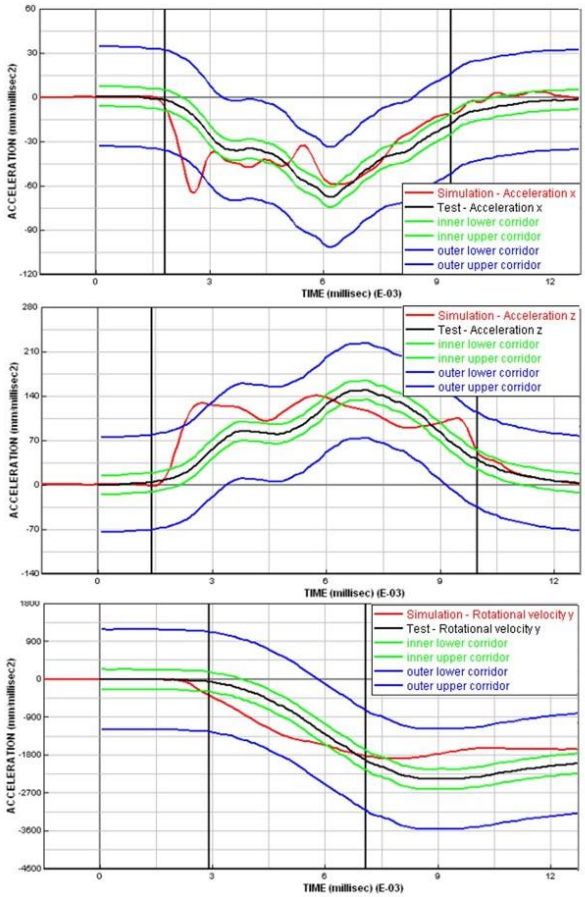

No.	Name				Rating	Weight
1	Corridor Method				0.7284	0.5
2	Correlation method	Value	Rating	Weight	0.675	0.5
a	Cross correlation function	0.9483	0.9244	0.2		
b	Size	0.943	0.943	0.4		
c	Phase shift	0.0007	0.2823	0.4		
3	Combination of 1 and 2				0.7017	
	Overall Rating:	**0.7017**				

No.	Name				Rating	Weight
1	Corridor Method				0.5408	0.5
2	Correlation method	Value	Rating	Weight	0.6646	0.5
a	Cross correlation function	0.9578	0.9381	0.2		
b	Size	0.7852	0.7852	0.4		
c	Phase shift	0.0007	0.4074	0.4		
3	Combination of 1 and 2				0.6027	
	Overall Rating:	**0.6027**				

No.	Name				Rating	Weight
1	Corridor Method				0.6197	0.5
2	Correlation method	Value	Rating	Weight	0.5866	0.5
a	Cross correlation function	0.9795	0.9695	0.2		
b	Size	0.9818	0.9818	0.4		
c	Phase shift	0.0008	0.0	0.4		
3	Combination of 1 and 2				0.6032	
	Overall Rating:	**0.6032**				

Fig. A18. CORA ratings of the acceleration and rotational velocity curves: motocross helmet – frontal – 45° anvil.

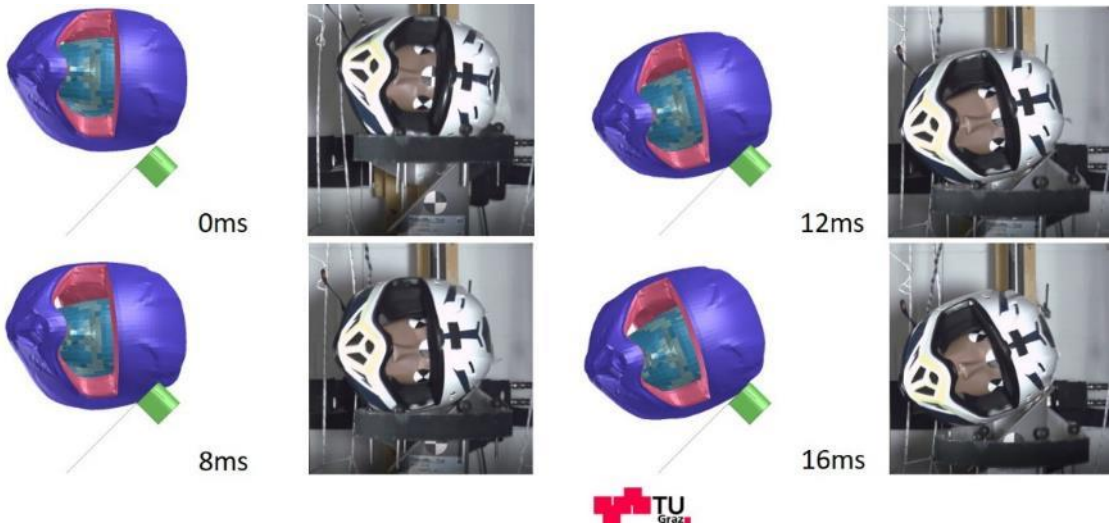

Fig. A19. Comparison of the kinematics: motocross helmet – side – 45° anvil.

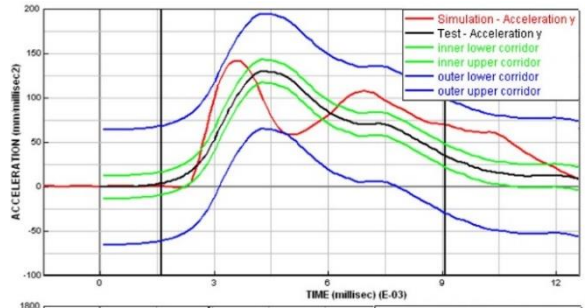

No.	Name				Rating	Weight
1	Corridor Method				0.5213	0.5
2	Correlation method	Value	Rating	Weight	0.8231	0.5
a	Cross correlation function	0.9382	0.9101	0.2		
b	Size	0.87	0.87	0.4		
c	Phase shift	0.0004	0.7327	0.4		
3	Combination of 1 and 2				0.6722	
	Overall Rating:	**0.6722**				

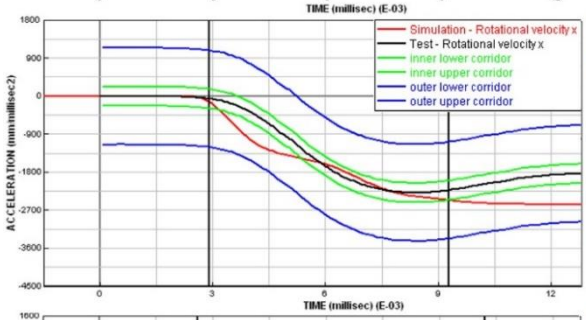

No.	Name				Rating	Weight
1	Corridor Method				0.8364	0.5
2	Correlation method	Value	Rating	Weight	0.6946	0.5
a	Cross correlation function	0.9923	0.9885	0.2		
b	Size	0.9671	0.9671	0.4		
c	Phase shift	0.0006	0.2751	0.4		
3	Combination of 1 and 2				0.7655	
	Overall Rating:	**0.7655**				

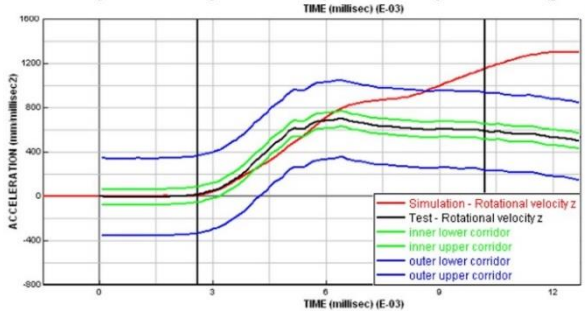

No.	Name				Rating	Weight
1	Corridor Method				0.5235	0.5
2	Correlation method	Value	Rating	Weight	0.3838	0.5
a	Cross correlation function	0.9857	0.9787	0.2		
b	Size	0.4702	0.4702	0.4		
c	Phase shift	-0.0009	0.0	0.4		
3	Combination of 1 and 2				0.4536	
	Overall Rating:	**0.4536**				

Fig. A20. CORA ratings of the acceleration and rotational velocity curves: motocross helmet – side – 45° anvil.

TABLE A1
CORA RESULTS OF THE HELMET VALIDATION

Load case	Curve	Full-face helmet	Motocross helmet
Rear – 0°	Acceleration X	0.5940	0.9183
	Acceleration Z	0.3971	0.7583
	Rotational velocity Y	0.4868	0.6868
Side – 0°	Acceleration Y	0.3907	0.7860
	Rotational velocity X	0.4982	0.7159
	Rotational velocity Z	0.8767	0.9505
Front – 0°	Acceleration X	0.3084	0.7633
	Acceleration Z	0.3596	0.8761
	Rotational velocity Y	0.6394	0.6371
Side – 45°	Acceleration Y	0.6651	0.6722
	Rotational velocity X	0.5617	0.7655
	Rotational velocity Z	0.6587	0.4536
Front – 45°	Acceleration X	0.6472	0.7017
	Acceleration Z	0.8263	0.6027
	Rotational velocity Y	0.6682	0.6032

TABLE A2
STANDARD CORA SETTINGS SPECIFIED IN VISUAL ENVIRONMENT

Corridor method	Maximal half width of inner corridor	0.1
	Maximal half width of outer corridor	0.5
Correlation method	Rating exponent for shape	3.0
	Rating exponent for size	1.0
	Rating exponent for phase	1.0

TABLE A3
COMPARISON OF INJURY CRITERIA OF TEST AND SIMULATION: MOTOCROSS HELMET

	Injury criteria	Drop test	Simulation	Deviation	Deviation [%]
Rear – flat anvil	Peak acceleration	239	159	80	33
	HIC 15	2775	2647	128	5
	BrIC	0.3378	0.2525	0.0853	25
Lateral – flat anvil	Peak acceleration	253	182	71	28
	HIC 15	2342	2745	403	17
	BrIC	0.5459	0.5800	0.0341	6
Front – flat anvil	Peak acceleration	210	195	15	8
	HIC 15	1839	2428	589	32
	BrIC	0.4597	0.3329	0.1268	28
Front – 45° anvil	Peak acceleration	162	109	53	33
	HIC 15	919	1223	304	33
	BrIC	0.7599	0.5599	0.2	26
Lateral – 45° anvil	Peak acceleration	134	84	50	37
	HIC 15	675	752	77	11
	BrIC	0.7711	0.8624	0.0913	12

TABLE A4

COMPARISON OF INJURY CRITERIA OF TEST AND SIMULATION: FULL-FACE HELMET

	Injury criteria	Drop test	Simulation	Deviation	Deviation [%]
	Peak acceleration	180 g	159 g	21	12
Rear – flat anvil	HIC 15	1782	2330	548	31
	BrIC	0.3209	0.1731	0.1478	46
	Peak acceleration	230	167	62	27
Lateral – flat anvil	HIC 15	1933	2856	932	48
	BrIC	0.5835	0.5675	0.016	3
	Peak acceleration	165	187	22	13
Front – flat anvil	HIC 15	1247	2234	987	79
	BrIC	0.5967	0.3927	0.204	34
	Peak acceleration	154	125	29	19
Front – 45° anvil	HIC 15	970	1269	299	31
	BrIC	0.728	0.5332	0.1948	27
	Peak acceleration	107	121	14	13
Lateral – 45° anvil	HIC 15	492	939	447	91
	BrIC	0.7507	0.7768	0.0261	3